

Electron-density dependence of double-plasmon excitations in simple metals

S. Huotari,¹ C. Sternemann,² W. Schülke,² K. Sturm,³ H. Lustfeld,³

H. Sternemann,² M. Volmer,² A. Gusarov,⁴ H. Müller,¹ and G. Monaco¹

¹*European Synchrotron Radiation Facility, Boîte Postale 220, F-38043 Grenoble cedex 9, France*

²*Fakultät Physik/DELTA, Technische Universität Dortmund, D-44221 Dortmund, Germany*

³*Institut für Festkörperforschung, Forschungszentrum Jülich GmbH, D-52425 Jülich, Germany*

⁴*SCK-CEN, Belgian Nuclear Research Centre, Boeretang 200, B-2400 Mol, Belgium*

(Received 4 March 2008; published 29 May 2008)

Double plasmons are unique fingerprints of dynamical correlations in the model of a free-electron gas beyond the random phase approximation. A combined experimental and theoretical study of double-plasmon excitations in three simple metals Na, Mg, and Al is presented. The intensities, spectral shapes, and dispersions of these excitations are analyzed as a function of momentum. The measured double-plasmon intensity is found to increase with a decreasing electron density, which is in good agreement with the expectations of strength of the correlation effects as a function of the electron gas density. The overall quantitative agreement between the experimental and the theoretical results is very good, while the remaining discrepancies may be due to higher order correlation effects and band-structure effects.

DOI: [10.1103/PhysRevB.77.195125](https://doi.org/10.1103/PhysRevB.77.195125)

PACS number(s): 78.70.Ck, 71.10.Ca, 71.45.Gm

I. INTRODUCTION

Electronic correlations in many-electron systems are a significant challenge to modern physics. While in strongly correlated systems their effect has to be considered from the outset,^{1,2} in simple metals a qualitative understanding can be derived from the model of a free-electron gas (FEG) within the random phase approximation³ (RPA). The RPA is valid in the high-density limit, i.e., $r_s \ll 1$, where r_s is an inverse density parameter defined by $(r_s a_0)^3 = 3/4\pi n$, n being the electron density, and a_0 the Bohr radius. Simple metals such as Al ($r_s = 2.07$), Mg ($r_s = 2.66$), and Na ($r_s = 3.93$) are the closest realizations of a FEG in nature because their crystal potentials can be treated as small perturbations to the FEG. However, the importance of the correlation effects beyond the RPA is expected to increase with the decreasing density, i.e., with increasing r_s . Since the valence electron densities of all elemental metals correspond to $r_s > 1$, the correlation effects are essential for a better qualitative and quantitative understanding of the dynamic response of metals.⁴

One of the canonical applications of the studies of the correlation effects in a many-electron system is the dynamics of valence electrons in a nearly free-electron gas. The corresponding fundamental excitation experimentally observed in a simple metal at a small momentum transfer is the plasmon,^{5–8} which is a collective excitation of the valence electrons caused by the long range Coulomb interaction and qualitatively understood within the RPA of the FEG.

Experimentally, the plasmon at finite momenta can be investigated by inelastic x-ray scattering⁹ (IXS) or electron-energy-loss spectroscopy¹⁰ (EELS). In both cases, the scattering cross section is proportional to the dynamic structure factor $S(\mathbf{q}, \omega)$, where \mathbf{q} is the momentum and ω is the energy transferred to the electron system under study. In many experiments, the attention has been focused on the plasmon dispersion^{5,6,11} but, especially in systems not resembling the FEG, the fine structure of the $S(\mathbf{q}, \omega)$ gives important information on many-body and band-structure-related effects.^{12–17}

However, even when applied to the FEG, the RPA cannot explain, for example, the finite linewidth, which is found to increase with the increasing $q = |\mathbf{q}|$ (Refs. 18 and 19), or the exact dispersion relation of the plasmon, especially in certain anomalies such as the negative dispersion in cesium.^{5,7,8,11,20} While for $q \rightarrow 0$, the observed small shift of the plasmon energy compared to its RPA value is due to the band-structure effects and core polarization, the increase in linewidth with an increasing q is a combined effect of the crystal potential and dynamical correlations, as has been demonstrated for Al.²¹ By studying the more detailed fine structure of the plasmon lineshape, it was also predicted that the so-called double-plasmon excitations (henceforth labeled as pl-pl) should cause an additional peaklike structure on the high energy side of the plasmon line.²¹ While its spectral weight was predicted to be vanishingly small for $q \rightarrow 0$, it should increase with the increasing q to the extent that the pl-pl excitations should be experimentally observable as a unique fingerprint of dynamical correlations. Indeed, the existence of the pl-pl excitations in Al has recently been clearly demonstrated to be in very good agreement with the theory.²²

The double-plasmon excitations have also been sought for by EELS studies.^{23,24} In EELS, the extrinsic multiple-scattering events overlap with the pl-pl excitations and their contribution has to be extracted based on the estimates of multiple-scattering probability, which can make the analysis difficult. Furthermore, the momentum dependence of the excitations could not be analyzed in detail. The IXS is a complementary probe of these excitations not suffering from the extrinsic multiple-scattering and is also applicable at large q , making it an excellent candidate for the studies of the pl-pl excitations. The complementary information obtained from the IXS can also serve as a necessary cross check for the accuracy of multiple-scattering corrections in EELS. More interestingly, however, hard x-ray scattering offers the possibility to study the dynamic response of electrons in extreme conditions such as high pressure.

In this paper, we report on the experimental results of the dependence of pl-pl excitations in Na, Mg, and Al on mo-

momentum transfer and electron density, and compare the results to the theory. The article is arranged as follows. The experimental details are outlined in Sec. II and the theoretical treatment is reviewed in Sec. III. Section IV presents the results and discussion. Finally, the conclusions are drawn in Sec. V. Atomic units (a.u.) are used throughout the paper with $\hbar=e=m=a_0=1$.

II. EXPERIMENT

The experiment was performed at the European Synchrotron Radiation Facility beamline ID16. The radiation from three consecutive undulators was monochromatized to a bandwidth of 1.3 eV with a double-crystal cryogenically cooled Si(111) monochromator. The spectra were measured using a Rowland-circle spectrometer in a backscattering geometry with a Johann-type analyzer crystal, which was a bent Si(555) wafer with a bending radius of $R=1$ m. The scattered photon energy was kept at 9.89 keV and the incident photon energy was tuned to measure the scattering cross section. The total energy resolution was set to 1.5 eV (full width at half maximum) (FWHM). The samples were polycrystalline Mg, Na, and single-crystalline Al. Part of the results for Al have been published earlier.²² The Al samples were 0.4 mm thick single crystals aligned so that it was possible to measure the energy-loss spectra with the momentum transfer vector parallel to the [110] and [100] directions. The Mg sample was a 0.7 mm thick polycrystalline pellet. Both Al and Mg samples were measured in a vacuum vessel at a pressure of 1 mbar to reduce the background scattering from the air. Due to its high reactivity, the polycrystalline Na sample was prepared in an Ar atmosphere and kept in a vacuum of 10^{-6} mbar during the experiment. The Na sample thickness was 0.5 mm and the spectra were taken in the transmission mode. All sample thicknesses correspond to roughly one absorption length of the 9.89 keV x-rays used in the experiment. The dynamic structure factors were measured by keeping the analyzer fixed and tuning the incident photon energy in the range of 0–100 eV energy transfers.

To study the possible contribution of multiple scattering, the measurement of Na for the momentum transfer $q=0.49$ a.u. was done by using sample thicknesses 0.5 and 0.1 mm. Both spectra were found to be identical, as shown in Fig. 1, confirming that in IXS experiments, the contribution of multiple scattering to the results presented here is negligible.

The dynamic structure factors were extracted from the measured spectra by (i) subtracting a small constant background measured with an empty cell, (ii) subtracting the quasielastic line tail, and (iii) normalizing the so obtained experimental $S_{\text{exp}}(q, \omega)$ using an extrapolation of the valence electron spectra above the $L_{2,3}$ edges and then employing the f -sum rule. The pl-pl peaks were extracted from the continuously decreasing main plasmon line by fitting a sum of Pearson VII (Ref. 25) and an exponential function to the plasmon tail and subtracting it from the data. An example of such a fit is presented in Fig. 1.

III. THEORY

The theory has been formulated in detail in Ref. 21, where the dynamical correlation up to the second order in the

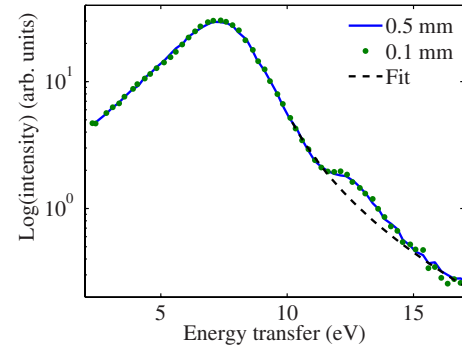


FIG. 1. (Color online) The spectra for Na at $q=0.49$ a.u. measured with two different sample thicknesses. It can be seen that the spectra are identical, confirming that the multiple-scattering contribution plays a negligible role in the double-plasmon feature. The fit to interpolate the main plasmon tail underlying the pl-pl peak is shown as a dashed line.

screened Coulomb interaction was shown to give rise to the plasmon-plasmon (pl-pl), particle-hole-pair-plasmon (ph-pl), and particle-hole-particle-hole pair (ph-ph) excitations. Since the theory applies to FEG, the response functions below depend on the magnitude but not on the direction of q . The dynamic structure factor $S(q, \omega)$ is related to the longitudinal dielectric function $\epsilon(q, \omega)$ by

$$S(q, \omega) = \frac{q^2}{4\pi^2 n} \text{Im}[-1/\epsilon(q, \omega)]. \quad (1)$$

Here, the dielectric function $\epsilon(q, \omega)$, in turn, is expressed in terms of the proper polarizability function $\pi_p(q, \omega)$ by

$$\epsilon(q, \omega) = 1 + v(q)\pi_p(q, \omega), \quad (2)$$

where $v(q)$ is the Coulomb potential. In many-body perturbation theory, $\pi_p(q, \omega)$ is expanded in terms of the irreducible polarizability diagrams, i.e.,

$$\pi_p(q, \omega) = \pi_0(q, \omega) + \pi_A(q, \omega) + \pi_B(q, \omega) + \pi_C(q, \omega) + \dots, \quad (3)$$

where $\pi_0(q, \omega)$ denotes the well-known RPA bubble, the $\pi_A(q, \omega)$ and $\pi_B(q, \omega)$ diagrams are of the first order, and the $\pi_C(q, \omega)$ is of the second order in the dynamically RPA-screened Coulomb potential.²¹ The corresponding diagrams are shown in Fig. 2, in which $\pi_A(q, \omega)$ is related to diagram (a), $\pi_B(q, \omega)$ to diagrams (b) and (c), and $\pi_C(q, \omega)$ to diagrams (d) and (e). The pl-pl excitations arise from the dynamic screening in the C diagrams only. The pl-pl contribution to the dynamic structure factor

$$S_{\text{theory}}^{\text{pl-pl}}(q, \omega) \propto \text{Im}[\pi_C^{\text{pl-pl}}(q, \omega)] \quad (4)$$

is calculated using the method of Ref. 21 for the three different valence electron densities corresponding to the metals Al, Mg, and Na. The spectral contribution of $S^{\text{pl-pl}}(q, \omega)$ to the total structure factor $S(q, \omega)$ is limited to a small energy range and, thus, gives rise to a peaklike structure that can be distinguished from the ph-pl excitations. Note that the pl-pl peak in $\text{Im}[\pi_C^{\text{pl-pl}}(q, \omega)]$ is the result of integrating pl-pl excitations over the internal energy and momentum variables.²²

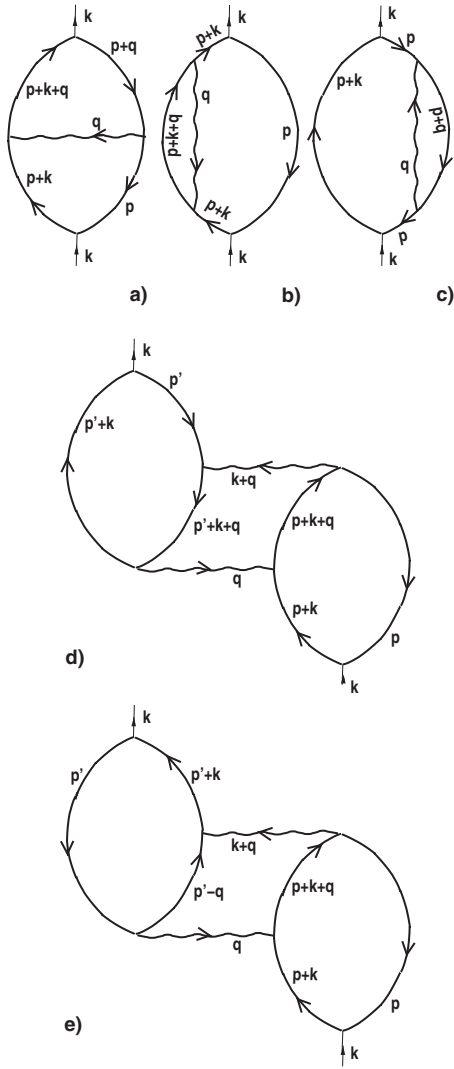


FIG. 2. The self-consistent subset of the interaction diagrams that were taken into account in the calculations (Ref. 21). The diagrams (a)–(c) are of the first order in the dynamically screened Coulomb interaction (wiggly line). The pl-pl excitations are due to the diagrams (d) and (e), which are of the second order in the screened Coulomb interaction.

Although the diagrams A, B, and C form a consistent subset,²⁶ there are further diagrams of the second order.^{27,28} Most of them represent corrections to the Green's functions or RPA corrections to the Coulomb interaction. The skeleton diagrams, i.e., those that do not belong to those classes, are depicted in Fig. 3. Within this study, we also performed calculations for Al at certain values of q from the contribution of the diagrams in Fig. 3 to $S(q, \omega)$, as far as double-plasmon excitations are concerned. However, contrary to the C diagrams,²² we find that the RPA screening yields, after integration over two internal energy variables, in all cases, products of the form

$$\epsilon_L^{-1}(k, \varepsilon) \epsilon_L^{-1}[|\mathbf{p} - \mathbf{p}' + \mathbf{k}|, -\omega - \varepsilon - E(\mathbf{p} + \mathbf{q} + \mathbf{k}) - E(\mathbf{p}' - \mathbf{k})], \quad (5)$$

where ϵ_L is the Lindhard dielectric function. \mathbf{k} , \mathbf{p} , \mathbf{p}' , and ε are the internal momentum and energy variables, with each

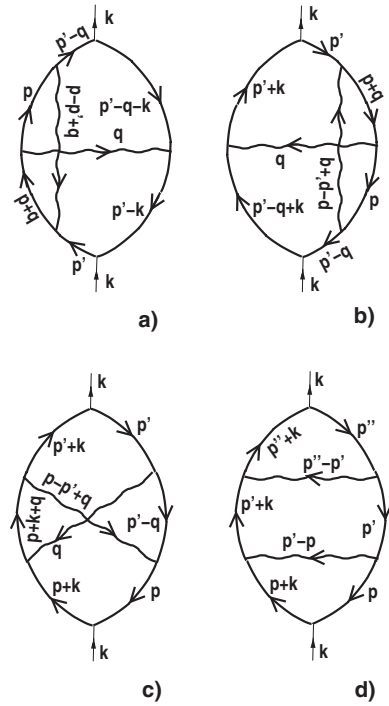


FIG. 3. All diagrams of the second order in the dynamically screened Coulomb interaction, which were not considered in Fig. 2. Those diagrams that merely represent corrections to the Green's functions or RPA corrections to the Coulomb interaction are not considered.

one to be integrated over. $E(\mathbf{p})$ is the kinetic energy of an electron with the momentum \mathbf{p} . The poles of the two involved screening functions indeed give rise to the excitations at

$$\omega = \omega^{\text{pl}}(k) + \omega^{\text{pl}}(|\mathbf{p} - \mathbf{p}' + \mathbf{k}|) + E(\mathbf{p} + \mathbf{q} + \mathbf{k}) - E(\mathbf{p}' - \mathbf{k}). \quad (6)$$

However, the integration over the three internal momentum variables and the inclusion of the corresponding kinetic energy variables into the energy argument of ϵ_L lead to excitation energies widely spread over the energy-loss scale. Therefore, the contribution of the diagrams shown in Fig. 3 were found to result in a smooth background in the vicinity of the pl-pl peak and, thus, affect only little the pl-pl excitations obtained from the C diagrams. For this reason, it is justified to subtract a smooth background function from the experimental $S(q, \omega)$ to obtain the pl-pl peak induced by the C diagrams.

It should be noted that this pl-pl peak is not related to the double-peak structure observed in several systems already in early IXS experiments, probing the particle-hole continuum with momentum transfers $q \sim 2q_c$.²⁹ That structure has, in fact, been shown to be induced by the band-structure effects.^{30–33}

IV. RESULTS AND DISCUSSION

The set of measured spectra from the three different metals is presented in Fig. 4. The results for Al have been pub-

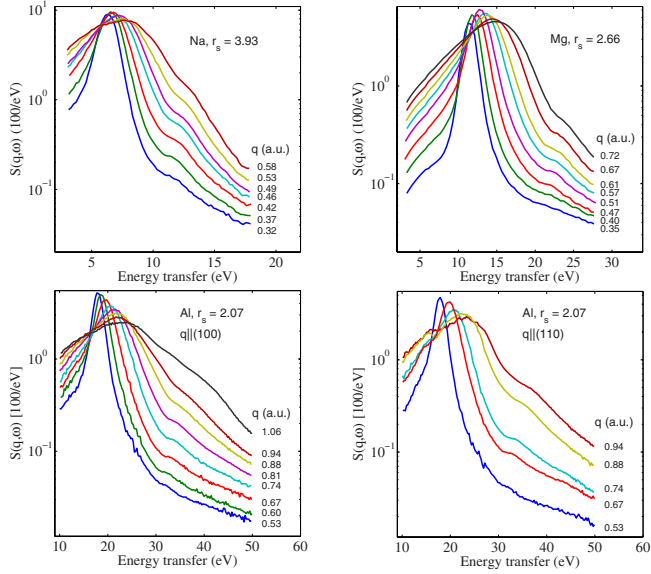


FIG. 4. (Color online) The measured dynamic structure factor of polycrystalline Na, Mg, and single-crystalline Al with $\mathbf{q} \parallel [100]$ and $\mathbf{q} \parallel [110]$ around the critical momentum q_c .

lished earlier and are reproduced here for comparison.²² All spectra are dominated by a single peak around the plasmon energy $\omega^{\text{pl}}(q)$. In all cases, there is also a small shoulder roughly at $2\omega^{\text{pl}}(q)$, which disperses and broadens with an increasing momentum transfer. This is assigned to a pl-pl excitation peak,²² on which we shall concentrate our analysis. In Al, the pl-pl excitation peak was studied with both $\mathbf{q} \parallel [100]$ and $\mathbf{q} \parallel [110]$. Whereas the main plasmon lineshapes in these two directions considerably differ from each other, the extracted pl-pl excitation peak was found to have a negligible orientation dependence.²² This suggests that the band-structure-related effects play a minor role in the pl-pl excitations.²¹ This is plausible for two reasons: (i) the band-structure effects are of higher order in the pl-pl excitations and (ii) any directional dependence is reduced due to the fact that the pl-pl peak consists of several pl-pl excitations.²¹

Since the only parameter needed to characterize a free-electron gas is its density parameter r_s , in principle, the strength of the correlation and the relative pl-pl peak intensity are directly related only to r_s , neglecting for the moment any effects due to the electron-ion interaction. In the limit of $r_s \rightarrow 0$ (high density), the electron gas should appear as uncorrelated, causing the probability of the intrinsic pl-pl excitations to vanish. From the samples measured in this study, the electron density is highest in Al and lowest in Na. It would, thus, be expected that the pl-pl excitation should be strongest in Na and weakest in Al, which is indeed observed in the experiment. Table I lists the relevant physical constants of the studied materials. The values for the critical cutoff momenta q_c were calculated within RPA. At q_c , the second zero crossing of the real part of the RPA dielectric function coincides with the high- ω edge of its imaginary part.³⁴

Using the interpolation procedure described in Sec. II and Ref. 22, we subtracted the main plasmon backgrounds from the pl-pl peaks. The obtained experimental pl-pl peaks with

TABLE I. Values for the electron-gas density parameter r_s , plasmon cutoff momenta q_c , and Fermi momenta k_F for the three studied sample materials.

	Na	Mg	Al
r_s	3.93	2.66	2.07
k_F (a.u.)	0.49	0.72	0.93
q_c (a.u.)	0.46	0.58	0.68

the theoretical predictions for Na, Mg, and Al(100) are shown in Fig. 5. The theoretical curves are convoluted with the experimental resolution function, i.e., a Gaussian with 1.5 eV FWHM. The lineshape found in the experiments is in good agreement with the theoretical prediction. Also, for the small momentum transfer values, the predicted pl-pl intensity is very close to the experimental observation. The energies of the measured excitations are very close to the theoretical results but, independently of the system studied, are always $\sim 10\%$ lower in the experiment than in the theory. Typically, the band-structure-related effects and the core-hole

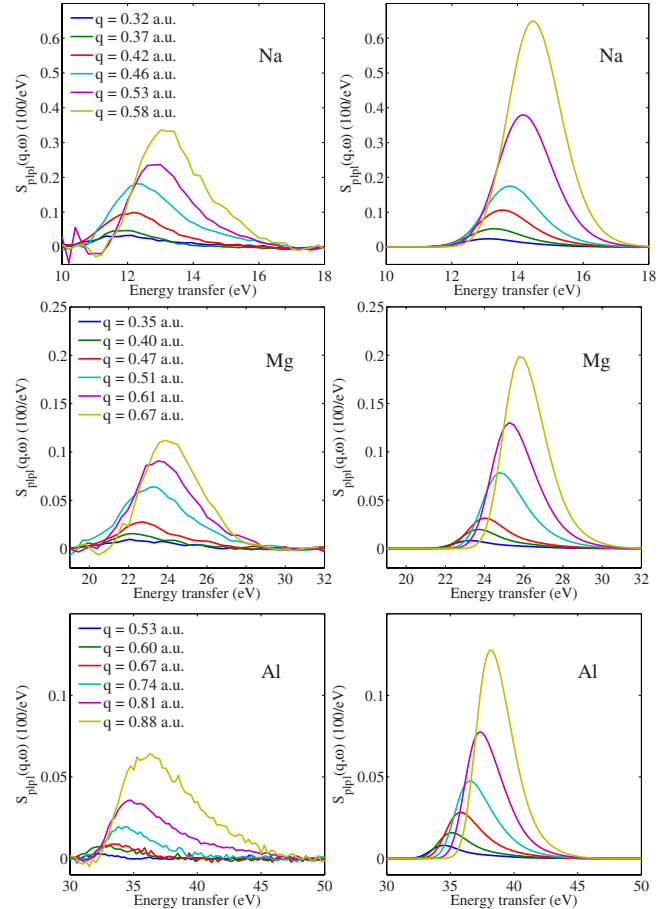


FIG. 5. (Color online) The pl-pl excitations for the selected momentum transfers measured in the three metals extracted from the main plasmon tail (left column) and the corresponding theoretical predictions (right column). The experimental result for Al refers to the orientation with $\mathbf{q} \parallel [100]$, the result for $\mathbf{q} \parallel [110]$ being the same within the present experimental accuracy. The highest maxima correspond to the highest momentum transfer values.

TABLE II. Theoretical and observed plasmon and pl-pl energies, and dispersion constants, measured and corrected for finite-resolution effects as described in the text.

	Na	Mg	Al
$\omega_{\text{RPA}}^{\text{pl}}(0)$ (eV)	6.05	10.9	15.8
$\omega_{\text{exp}}^{\text{pl}}(0)$ (eV)	5.74	10.4	15.1
$\omega_{\text{theory}}^{\text{pl-pl}}(0)$ (eV)	12.2	21.8	32.4
$\omega_{\text{exp}}^{\text{pl-pl}}(0)$ (eV)	10.7	20.9	29.8
$\alpha_{\text{RPA}}^{\text{pl}}$	0.32	0.39	0.44
$\alpha_{\text{exp}}^{\text{pl}}$	0.21	0.34	0.37
$\alpha_{\text{theory}}^{\text{pl-pl}}$	0.22	0.25	0.27
$\alpha_{\text{exp}}^{\text{pl-pl}}$	0.23	0.22	0.29

polarizability are known to shift the plasmon energy to slightly lower values and could also affect the pl-pl excitations, which would explain the observed difference.

The main results of the study are collected in Tables II and III. They list all the parameters obtained from the plasmon and pl-pl data, namely their positions, dispersions, and ω -integrated intensities, both for experimental results and the predictions by the theory described in Ref. 21. The plasmon energies $\omega^{\text{pl}}(0)$ and the dispersion constants α^{pl} , which are based on RPA, are compared to the experimental values for the main plasmon line. The experimental plasmon energies $\omega^{\text{pl}}(q=0)$ and the dispersion constants α^{pl} were obtained by fitting both the experimental and theoretical $\omega^{\text{pl}}(q)$ to a quadratic dispersion law,

$$\omega^{\text{pl}}(q) = \omega^{\text{pl}}(0) + \alpha^{\text{pl}}q^2. \quad (7)$$

Likewise, the double-plasmon energies were obtained by fitting for the peak position the law

$$\omega^{\text{pl-pl}}(q) = \omega^{\text{pl-pl}}(0) + \alpha^{\text{pl-pl}}q^2. \quad (8)$$

To study the dispersion of the pl-pl peak, one has to consider that due to the broadening caused by the finite experimental resolution in both the energy and momentum transfer, and due to the asymmetric pl-pl lineshape, the experimentally observed peak position differs from the intrinsic one. From the theoretical pl-pl lineshape of Na, it can be inferred that a measurement with a finite energy resolution of 1.5 eV shifts its peak position by ~ 0.34 eV toward higher energies. This correction was done to the experimental data to get the parameter $\omega^{\text{pl-pl}}(0)$ reported in Table II. The corresponding

TABLE III. Theoretical and observed pl-pl intensities. $I(q)$ is the relative intensity of the pl-pl peak with respect to the integrated intensity of $S_{\text{exp}}(q, \omega)$. In this table, it is evaluated both at the Fermi wave vector k_F and at q_c .

	Na	Mg	Al
$I_{\text{theory}}(q_c)$ (%)	0.90	0.49	0.35
$I_{\text{exp}}(q_c)$ (%)	1.0 ± 0.1	0.4 ± 0.1	0.2 ± 0.1
$I_{\text{theory}}(k_F)$ (%)	1.11	1.04	1.12
$I_{\text{exp}}(k_F)$ (%)	1.0 ± 0.1	0.6 ± 0.1	0.6 ± 0.1

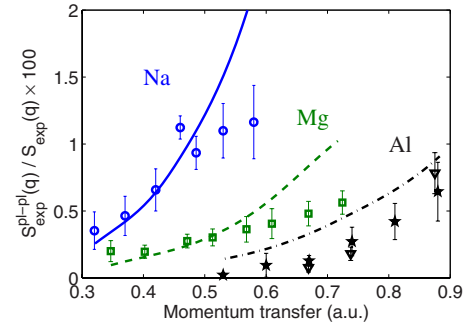


FIG. 6. (Color online) The intensity of the pl-pl peak with respect to the intensity of the $S_{\text{exp}}(q, \omega)$ in the three metals. The solid, dashed, and dash-dotted lines refer to the theoretical results for Na, Mg, and Al (Ref. 22), respectively. The experimental results are depicted by circles (Na), squares (Mg), stars (Al[100]), and triangles (Al[110]). The error bars refer to the systematic uncertainty due to the involved fitting procedure.

correction for Mg is 0.33 eV and for Al, it is 0.49 eV. This correction is justified since the pl-pl lineshapes of the convoluted theory and experimental results appear to be in good agreement. It can be seen from the results of Table II that the agreement between the experimental and the theoretical values is very good. However, some discrepancies remain, most obviously in the values for the pl-pl peak position, as discussed above. The RPA plasmon dispersion coefficients $\alpha_{\text{RPA}}^{\text{pl}}$ are well known to overestimate the experimentally observed values (e.g., see Ref. 11), which is reproduced in our results in Table II. However, the dispersion coefficients of the pl-pl excitations seem to be in very good agreement with the theoretical prediction for all the studied samples, confirming the accuracy of the theoretical treatment.

The relative ω -integrated intensity of the pl-pl peak $I(q) = S^{\text{pl-pl}}(q)/S_{\text{exp}}(q)$ is reported in Fig. 6 as a function of q , and, in Table III, is evaluated at q_c and k_F . The $S_{\text{exp}}(q) = \int_0^\infty S_{\text{exp}}(q, \omega) d\omega$ is the total intensity of the experimentally measured spectrum. The overall agreement, especially as a function of the electron density, is good. Both the experiment and the theory confirm that the largest pl-pl contribution is for Na (largest r_s) and the smallest is for Al (smallest r_s). However, certain disagreements between the experiment and the theory exist in Fig. 6. First of all, for small values of momentum transfer, the agreement between the experiment and the theory is very good in the case of Na and Mg, but for Al, the theory overestimates the intensity by a factor of roughly two, as reported earlier.²² Second, the theory predicts a larger increase in intensity toward large q than is observed in the experiment, where the q dependence is smaller and the intensity seems to even reach a plateau above q_c . Since the pl-pl excitation can only exist between $0 < q < 2q_c$, it would be expected to become weaker toward $q=2q_c$. However, since it simultaneously merges into the particle-hole continuum, it cannot be adequately described by the calculation scheme of Sturm and Gusarov,²¹ which is only valid outside the particle-hole continuum. Moreover, the extraction of the pl-pl excitations from the experimental data is increasingly difficult beyond $\sim 1.5q_c$ and the values start to be sensitive to the exact data analysis method. Another ex-

planation might be that, since, with an increasing q , shorter-range interactions are probed, this discrepancy between the theory and the experiment at large q is due to an incomplete description of the short-range correlation effects in the theory.

V. CONCLUSIONS

Double-plasmon excitations were studied in three different free-electron-like metals spanning the typical electron-density range found in solids. The results confirm that the pl-pl excitation is a universal property of the electron gas and can be observed in several metallic solid-state systems. The electron-density dependence was observed to behave as predicted, i.e., the pl-pl excitation peak increases with the decreasing electron density. While the plasmon lineshape in Al depends on the crystallographic direction, the extracted pl-pl

excitation was found to be isotropic, confirming that it is not largely affected by the band-structure effects. The experimentally found intensities are very well reproduced by the theory with small discrepancies emerging in the high-density and high- q limits. The discrepancies may be related to a higher-order correlation that was not taken into account in the theoretical treatment. The results give an important testing ground for the calculations of the screened electron-electron interaction and the many-body effects in a free-electron gas.

ACKNOWLEDGMENTS

We are grateful to G. Vankó for his help during the experiments and for the critical discussions, R. Verbeni for his help in preparing and performing the experiments, and C. Henriquet for his expert technical assistance. M. Tolan is gratefully acknowledged for his support.

-
- ¹E. Dagotto, *Science* **309**, 257 (2005).
²V. I. Anisimov, F. Aryasetiawan, and A. I. Lichtenstein, *J. Phys.: Condens. Matter* **9**, 767 (1997).
³D. Pines, *Elementary Excitations in Solids* (Benjamin, New York, 1963).
⁴G. D. Mahan, *Many-Particle Physics*, 3rd ed. (Plenum, New York, 2000).
⁵A. vom Felde, J. Sprösser-Prou, and J. Fink, *Phys. Rev. B* **40**, 10181 (1989).
⁶J. Sprösser-Prou, A. vom Felde, and J. Fink, *Phys. Rev. B* **40**, 5799 (1989).
⁷A. Fleszar, R. Stumpf, and A. G. Eguiluz, *Phys. Rev. B* **55**, 2068 (1997).
⁸F. Aryasetiawan and K. Karlsson, *Phys. Rev. Lett.* **73**, 1679 (1994).
⁹W. Schülke, *Electron Dynamics by Inelastic X-Ray Scattering* (Oxford University Press, New York, 2007).
¹⁰J. Fink, *Adv. Electron. Electron Phys.* **75**, 121 (1989).
¹¹C. A. Burns, P. Giura, A. Said, A. Shukla, G. Vankó, M. Tuel-Benckendorf, E. D. Isaacs, and P. M. Platzman, *Phys. Rev. Lett.* **89**, 236404 (2002).
¹²H.-C. Weissker, J. Serrano, S. Huotari, F. Bruneval, F. Sottile, G. Monaco, M. Krisch, V. Olevano, and L. Reining, *Phys. Rev. Lett.* **97**, 237602 (2006).
¹³S. Galambosi, J. A. Soininen, A. Mattila, S. Huotari, S. Manninen, G. Vankó, N. D. Zhigadlo, J. Karpinski, and K. Hämäläinen, *Phys. Rev. B* **71**, 060504(R) (2005).
¹⁴S. Galambosi, J. A. Soininen, K. Hämäläinen, E. L. Shirley, and C.-C. Kao, *Phys. Rev. B* **64**, 024102 (2001).
¹⁵I. G. Gurtubay, J. M. Pitarke, W. Ku, A. G. Eguiluz, B. C. Larson, J. Tischler, P. Zschack, and K. D. Finkelstein, *Phys. Rev. B* **72**, 125117 (2005).
¹⁶J. Z. Tischler, B. C. Larson, P. Zschack, A. Fleszar, and A. G. Eguiluz, *Phys. Status Solidi B* **237**, 280 (2003).
¹⁷N. Hiraoka, H. Ishii, I. Jarrige, and Y. Q. Cai, *Phys. Rev. B* **72**, 075103 (2005).
¹⁸W. Ku and A. G. Eguiluz, *Phys. Rev. Lett.* **82**, 2350 (1999).
¹⁹K. Sturm and L. E. Oliveira, *Phys. Rev. B* **24**, 3054 (1981).
²⁰A. A. Quong and A. G. Eguiluz, *Phys. Rev. Lett.* **70**, 3955 (1993).
²¹K. Sturm and A. Gusarov, *Phys. Rev. B* **62**, 16474 (2000).
²²C. Sternemann, S. Huotari, G. Vankó, M. Volmer, G. Monaco, A. Gusarov, H. Lustfeld, K. Sturm, and W. Schülke, *Phys. Rev. Lett.* **95**, 157401 (2005).
²³J. C. H. Spence and A. E. C. Spargo, *Phys. Rev. Lett.* **26**, 895 (1971).
²⁴P. Schattschneider, F. Födermayr, and D.-S. Su, *Phys. Rev. Lett.* **59**, 724 (1987), and references therein.
²⁵H. Wang and J. Zhou, *J. Appl. Crystallogr.* **38**, 830 (2005).
²⁶D. J. W. Geldart and S. H. Vosko, *Can. J. Phys.* **44**, 2137 (1966).
²⁷A. J. Glick and W. F. Long, *Phys. Rev. B* **4**, 3455 (1971).
²⁸M. E. Bachlechner, A. Holas, H. M. Böhm, and A. Schinner, *Phys. Rev. B* **54**, 2360 (1996).
²⁹P. M. Platzman and P. Eisenberger, *Phys. Rev. Lett.* **33**, 152 (1974).
³⁰C. Sternemann, A. Kaprolat, and W. Schülke, *Phys. Rev. B* **57**, 622 (1998).
³¹W. Schülke, U. Bonse, H. Nagasawa, S. Mourikis, and A. Kaprolat, *Phys. Rev. Lett.* **59**, 1361 (1987).
³²A. Fleszar, A. A. Quong, and A. G. Eguiluz, *Phys. Rev. Lett.* **74**, 590 (1995).
³³B. C. Larson, J. Z. Tischler, A. Fleszar, and A. G. Eguiluz, *J. Phys. Chem. Solids* **61**, 391 (2000).
³⁴Note that in Ref. 22 a slightly different q_c value for Al was used.